Rochester Institute of Technology

RIT Digital Institutional Repository

Theses

2-2015

CMOS Compatible 3-Axis Magnetic Field Sensor using Hall Effect Sensing

Joshua R. Locke
jrl5111@rit.edu

Follow this and additional works at: https://repository.rit.edu/theses

Recommended Citation

Locke, Joshua R., "CMOS Compatible 3-Axis Magnetic Field Sensor using Hall Effect Sensing" (2015). Thesis. Rochester Institute of Technology. Accessed from

This Thesis is brought to you for free and open access by the RIT Libraries. For more information, please contact repository@rit.edu.

CMOS Compatible 3-Axis Magnetic Field Sensor using Hall Effect Sensing

By

Joshua R. Locke

A Thesis Submitted

In Partial Fulfillment

of the Requirements of the Degree of

MASTER OF SCIENCE

In Microelectronic Engineering

Approved by:

Professor ____ Date: _____________
Dr. Lynn F. Fuller (Thesis Advisor)

Professor ____ Date: _____________
Dr. Ivan Puchades (Thesis Committee Member)

Professor ____ Date: _____________
Dr. Santosh Kurinec (Thesis Committee Member)

Professor ____ Date: _____________
Dr. Robert Pearson (Director, Microelectronics Engineering Program)

Professor ____ Date: _____________
Dr. Sohail Dianat (Chair, Electrical and Microelectronics Engineering Department)

DEPARTMENT OF ELECTRICAL & MICROELECTRONIC ENGINEERING

KATE GLEASON COLLEGE OF ENGINEERING

ROCHESTER INSTITUTE OF TECHNOLOGY

ROCHESTER, NEW YORK

FEBRUARY 2015

TABLE OF CONTENTS

Material	Page
Acknowledgements	3
Abstract	4
Units for Magnetic Properties	5
Rationale	6
Theory	7
Objectives	11
Methods	12
Design	12
Fabrication	17
Packaging	22
Testing	23
Third Axis Design	28
Conclusion	32
References	33

Acknowledgments

I would like to thank my thesis advisor Dr. Lynn Fuller for his countless hours of support and guidance on my thesis work, without which this project could not have been completed. I would also like to thank all of the staff of the RIT Microelectronics Engineering Department including Dr. Ivan Puchades, for their invaluable recommendations and insight. Lastly, I would like to thank the staff of the RIT SMFL for assisting me in all processing and fabrication steps.

1. ABSTRACT

The purpose of this study is to design, fabricate and test a CMOS compatible 3-axis Hall effect sensor capable of detecting the earth's magnetic field, with strength's of ~50 μT. Preliminary testing of N-well Van Der Pauw structures using strong neodymium magnets showed proof of concept for hall voltage sensing, however, poor geometry of the structures led to a high offset voltage. A 1-axis Hall effect sensor was designed, fabricated and tested with a sensitivity of 1.12×10^{-3} mV/Gauss using the RIT metal gate PMOS process. Poor geometry and insufficient design produced an offset voltage of 0.1238 volts in the 1-axis design; prevented sensing of the earth's magnetic field. The new design features improved geometry for sensing application, improved sensitivity and use the RIT sub-CMOS process. The completed 2-axis device showed an average sensitivity to large magnetic fields of 0.0258 μV/Gauss at 10 mA supply current.

TABLE 1
UNITS FOR MAGNETIC PROPERTIES [4]

Symbol	Quantity	CGS Unit	Conversion	SI Unit
Φ	Magnetic Flux	Maxwell [Mx], G-cm^2	10^{-8}	Weber [Wb], V-sec
B	Magnetic Flux Density	Gauss [G]	10^{-4}	Tesla [T], Wb/m^2
U	Magnetomotive Force	Gilbert [Gb]	$10/4\pi$	Ampere [A]
H	Magnetic Field Strength	Oersted [Oe]	$10^3/4\pi$	A/m
M	Magnetization	emu/cm^3	10^3	A/m
$4\pi M$	Magnetization	G	$10^3/4\pi$	A/m
J	Magnetic Polarization	emu/cm^3	$4\pi \times 10^{-4}$	T, Wb/m^2
μ	Permiability	1	$4\pi \times 10^{-7}$	H/m, Wb/(A-m)
μ_r	Relative Permeability	-		-

erg = ergon

1 erg = 10^{-7} Joules

1 erg = 6.2415×10^{11} eV

1 erg/G = 1 emu

emu = electromagnetic unit

2. RATIONALE

The Hall effect was first observed and characterized in 1879 by Edwin Hall in various metal conductors. Since its discovery, Hall effect devices have been used as an efficient way of sensing that offers many advantages over similar technologies. Furthermore, semiconductors are highly suited for Hall effect measuring. This combined with the advances in modern semiconductor processing; Hall effect sensors have become one of the most popular solid-state transducers manufactured today. Traditionally, Hall effect devices are used to sense the strength of a magnetic field or the presence of a current. Other devices exist, such as magnetoresistors, Lorentz force sensors, fluxgate magnetometers and superconducting quantum interface devices; which can be used to sense magnetic fields, however, Hall devices offer a number of advantages over other designs. Some advantages of Hall devices include their relatively small size, durability and their ability to be made with traditional IC processes [9]. This has the added benefit of being able to include any circuitry needed to amplify or filter the sensors signal on the same chip as the sensor itself. Microelectromechanical systems (MEMS) based Hall effect sensors are very common in modern electronics. Common applications for Hall effect sensors include contactless position sensing, RPM sensing, timing measurement, pulse counters, current sensing, brushless motor control, and flow meters. A relatively new application of these sensors is 3-dimensional digital compassing (Magnetometer). For a magnetometer to function, the magnetic field must be capable of detecting the Earth's magnetic field of around 50 μT.

When a conductor is placed in the presence of a magnetic field, the charge carriers experience a Lorentz Force as given in equation 1 [8].

$$\vec{F} = q\vec{E} + q(\vec{v} \times \vec{B}) \quad \text{(equation 1)}$$

where q is the elementary charge of 1.6×10^{-19} Coulombs, the electric field E, carrier velocity v, and magnetic flux density B. Figure 1 shows a conductor of thickness t and width w. When a current, I_x, is passed through the conductor, the net flow of charges is in the x-direction. In the presence of a perpendicular magnetic flux, B_z, as seen in Figure 2, the charge carriers experience a Lorentz Force. This force pushes the carriers to one side of the conducting material creating a voltage potential across the material in the y-direction.

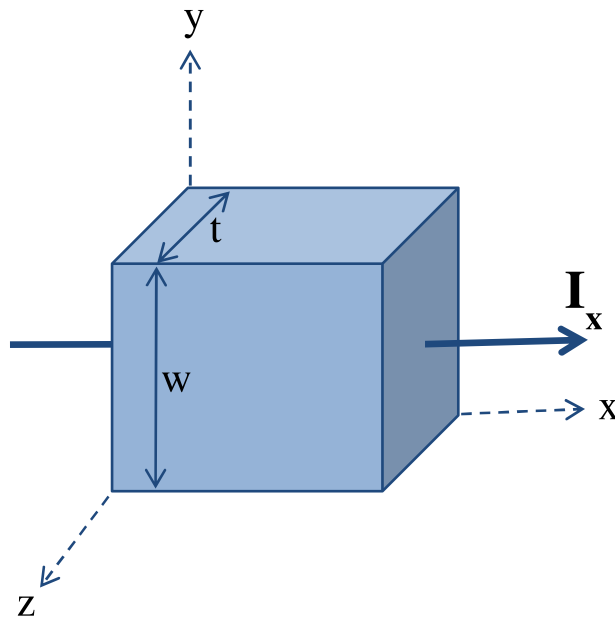

Figure 1: A sample material of thickness *t* and width *w*. A current (*I*) is passed through the material in the x-direction.

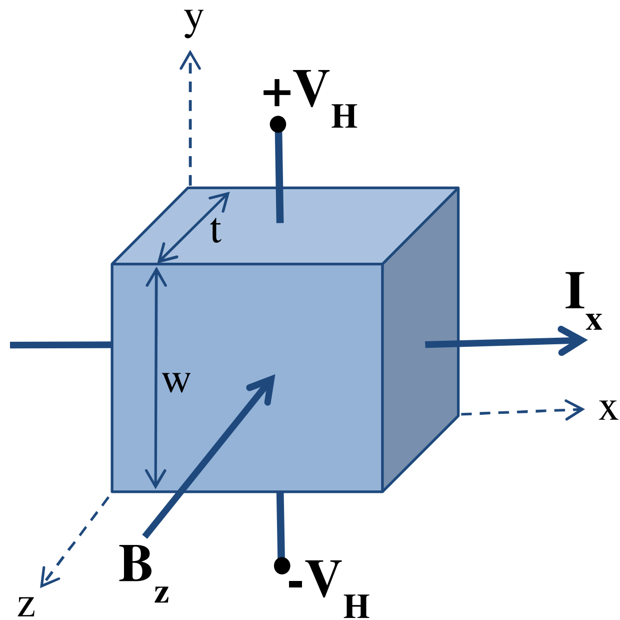

Figure 2: A sample material of thickness *t* and width *w*. A current I is passed through the material in the x-direction. In the presence of a magnetic field acting in the z-direction (90 degrees to the current flow) a voltage difference is generated across the conductor in the y-direction known as the Hall voltage.

It should be noted that all of these parameters are vector quantities and thus the sensitivity of the Hall device is very much dependant on the direction of the magnetic field into the conducting material. In a conductor, it has been shown that the magnitude of the Hall voltage produced is proportional to the current applied, the magnetic field strength and the amount of carrier density in the material as shown in equation 2.

$$V_H = \frac{IB}{qnt} \qquad \text{(equation 2)}$$

Where I is the applied current, B is the magnetic field strength, q is the electron charge, n is the carrier density and *t* is the thickness of the conductor. From equation 2, it is shown

that the Hall voltage produced is greatly dependant on the current through the device and the strength of the magnetic field and inversely proportional to the carrier density. Equation 2 also shows that a Hall effect device can be used to determine the strength of a magnetic field with a known current or the magnitude of the current can be determined in the presence of a known magnetic field. Since the carrier density in pure conductors, like a metal, are extremely high, the Hall voltage produced is small; making metals not practical materials for Hall effect devices. Table 2 shows the intrinsic carrier concentration for common materials at 300 K [6].

TABLE 2
INTRINSIC CARRIER CONCENTRATION AT 300 K

Material	Carrier Concentration [cm^{-3}]
Copper	$8.40x10^{22}$
Silicon	$1.50x10^{10}$
Germanium	$2.10x10^{12}$
Gallium-Arsenide	$1.10x10^{7}$

From Table 2 and equation 2, it can be seen that semiconductor materials make much more sensitive Hall effect devices than metals due to their naturally lower carrier concentrations. Semiconductors also make excellent materials for Hall effect devices because they must be doped with ions to become electrically active and depending on the dopant species, the majority carrier can be chosen as either electrons or holes. In equation 2, *nt* may be substituted with an implanted dose *Q* allowing for tuning of the device sensitivity. In the case of this experiment, electrons were chosen as the majority carrier as they tend to have a higher mobility than holes which gives the device slightly higher sensitivity to magnetic field changes. The Hall Coefficient (R_H) is a material dependent

property that shows the effectiveness of the Hall voltage generated with a given current and magnetic field strength applied. The Hall coefficient is measured in units of Ω - cm/Gauss, cm^3/coulomb or m^3/amp-sec. Equations 3 and 4 show how R_H is determined.

$$R_H = \frac{-V_H t}{IB} \qquad \text{(equation 3)}$$

$$R_H = \frac{-1}{qn} \qquad \text{(equation 4)}$$

Table 3 shows the Hall coefficient for different materials.

TABLE 3
HALL COEFFICIENT FOR MATERIALS

Material	R_H [$x10^{-12}$ Ω-cm/Gauss]
Aluminum	-0.39
Gold	-0.70
Copper	-0.50
Potassium	-4.20

The conductors in Table 3 have very low Hall coefficients due to the naturally larger intrinsic carrier concentrations. The Hall coefficient is not as simple in semiconductors as electron and hole mobilities must be considered. Equations 5 and 6 show how to calculate the Hall coefficient for a semiconductor where μ_e and μ_h are the electron and hole drift mobilities respectively [6].

$$R_H = \frac{p - nb^2}{q(p + nb)^2} \quad \text{(equation 5)}$$

$$b = \frac{\mu_e}{\mu_h} \quad \text{(equation 6)}$$

To see how effective semiconductors are as Hall devices, and using the Hall coefficient as a reference; take intrinsic silicon with an intrinsic carrier concentration (n_i) of 1.5×10^{10} cm^{-3} and taking μ_e = 1350 $cm^2V^{-1}s^{-1}$ and μ_h = 450 $cm^2V^{-1}s^{-1}$. Substituting into equations 5 and 6 gives a Hall coefficient of R_H=-208 $m^3A^{-1}s^{-1}$. Comparing this value to those in Table 3 shows that semiconducting materials are orders of magnitude greater at sensing the Hall voltage [2].

3. OBJECTIVES

The objective of this study is to design, fabricate and test a functioning Hall effect magnetic field sensor using the processes and tools available at RIT. The desired sensor will ideally have a high enough sensitivity to detect the Earth's magnetic field of approximately 50 µT. The design will ideally also have sensing capabilities in 3-axis.

4. METHODS

Design

There are many factors that can be optimized on a Hall device through design including the sensitivity, the output linearity, the offset voltage, noise canceling, and the temperature effect on sensitivity. Many of these must be optimized with on-chip circuitry and were not included in the design for this investigation. A simple “cross” configuration was used with the main parameter measured being the sensitivity [5]. The new design will consist of two separate 5mm x 5mm die, the first die being the X and Y directional sensing axis and the second die for the Z-axis sensing. Both chips will be CMOS compatible and packaged together as a single device. This will minimize process complexity and serve to isolate the 2-axis sensor design from the third axis. As such, both die were designed separately. The 2-axis design uses the RIT sub-CMOS Process for fabrication [3]. This RIT process uses modified MOSIS design rules with 11 lithography steps, a λ of 0.5 μm and an L_{min} of 1.0 μm. The 2-axis design will make use of only four lithography levels; n-well, channel stop, contact cuts and metal. Figure 3 shows the basic design of the new Hall sensor

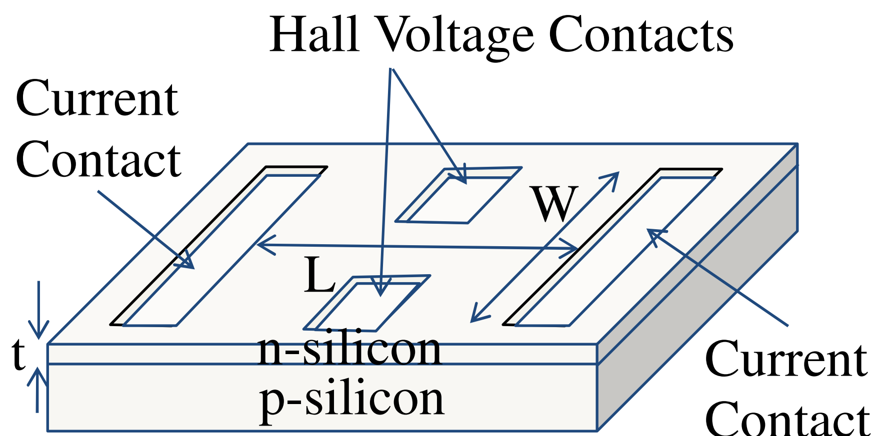

Figure 3: Hall Sensor design including current contacts and Hall voltage contacts. The sensor is built in an n-well on p-type silicon.

Some key notes about this design are that the entire sensor is built inside a lightly doped n-well to increase sensitivity of the device. Hall contacts were made small to minimize the offset voltage to as close to zero as possible. The two axis design consists of two Hall devices on a die with the same design. The y-axis sensing design is identical to the x-axis design but rotated 90 degrees so the current runs perpendicular to the first axis as seen in Figure 4.

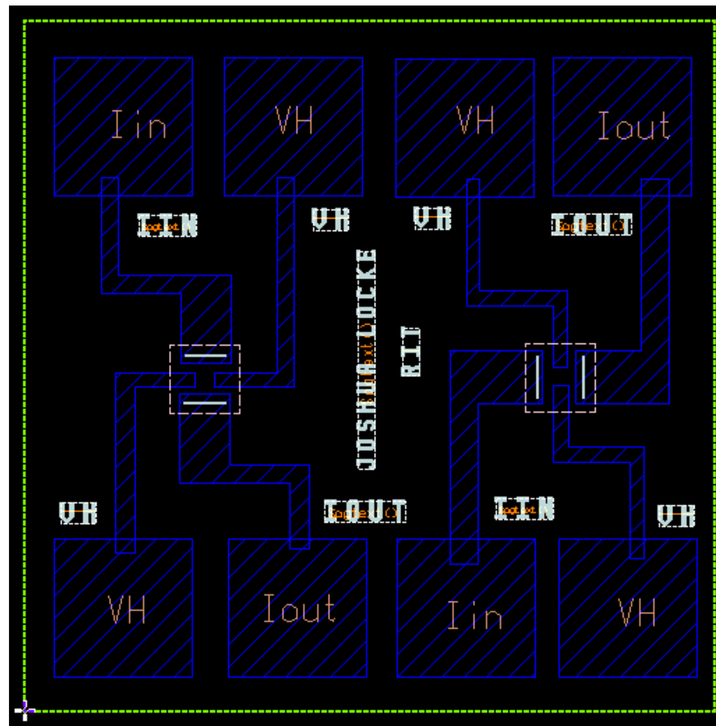

Figure 4: Mask layout of the designed 2-axis (x and y) Hall effect sensor. Layout shows entire chip (green dash), n-well (pink dash), contacts (solid grey) and metal (blue) layers.

Table 4 shows the designed device dimensions for all of the features. It should be noted that scaling of the device was not investigated so feature sizes are relatively large to

ensure successful fabrication and make packaging and testing easier. Theory states that if dimensional ratios remain the same, there should be no loss in sensitivity of the devices.

TABLE 4
2-AXIS HALL SENSOR DESIGN CONSIDERATIONS

Feature	Designed
Chip Size	5 mm x 5 mm
n-Well	500 μm x 500 μm
Current Contacts	300 μm x 10 μm
Hall Contacts	10 μm x 10 μm
Aluminum Pads	1 mm x 1 mm

The largest design consideration for any Hall device is the doping concentration as this determines the sensitivity of the sensor as seen in equation 2. For the proposed design, an n-well with a doping of Q = 9.5E12 cm^{-2} was implanted into the substrate. Substituting this dose Q into equation 2 gives a theoretical sensitivity of 0.0658 mV/G with 10 mA supply current and in the presence of Earth's magnetic field of approximately 0.5 Gauss. Figure 5 shows the expected Hall voltage output of this sensor design for given input currents.

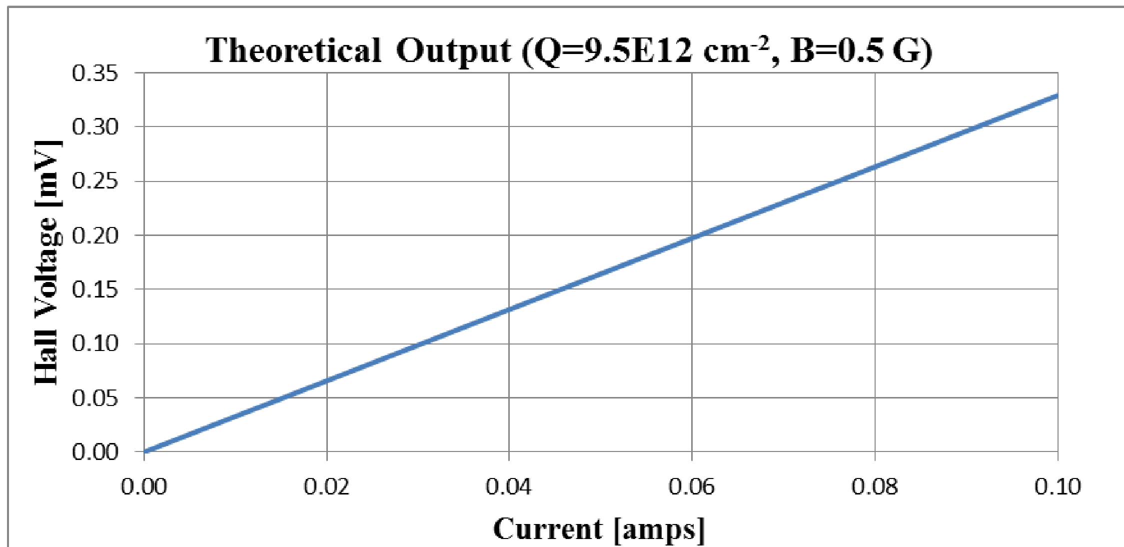

Figure 5: Hall sensor expected output with an implanted n-well dose of 9.5E12 cm^{-2} and magnetic field strength of 0.5 Gauss.

ATLAS and ATHENA were used to simulate the device fabrication in order to determine fabrication parameters. An early version of fabricated devices did not contain a channel stop implant to isolate the x and y axes from each other and as a result, these devices were shorted amongst each other and did not perform as expected. Figure 6 shows the results of a device with no channel stop.

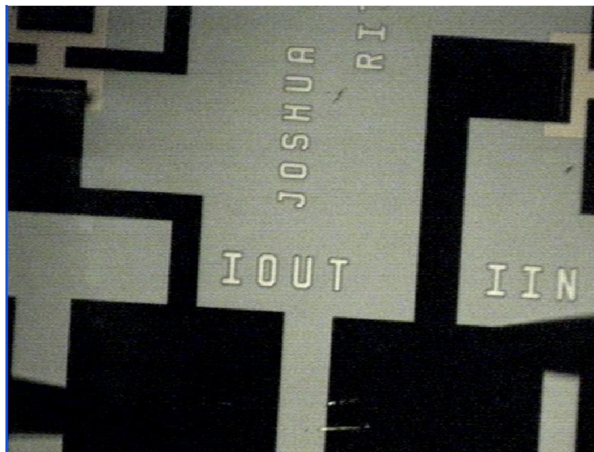

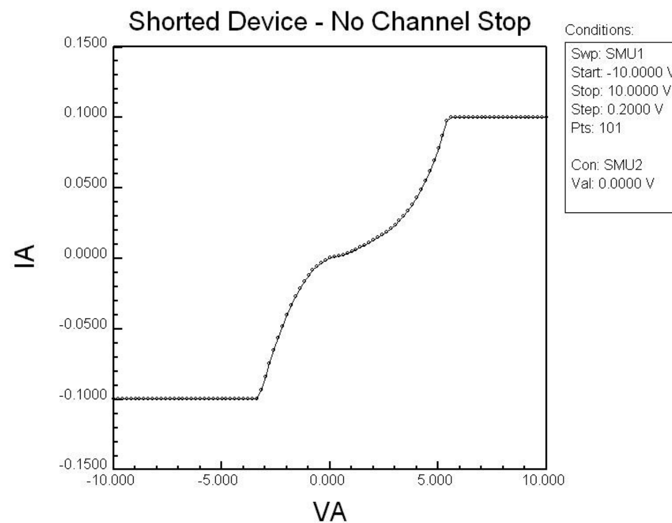

Figure 6: With no channel stop, the x and y axes are shorted when the voltage is swept between two probes connected on pads of the two axes (top). The voltage is swept from -10 to 10 volts and the current is measured using an HP4145 Analyzer test station (bottom).

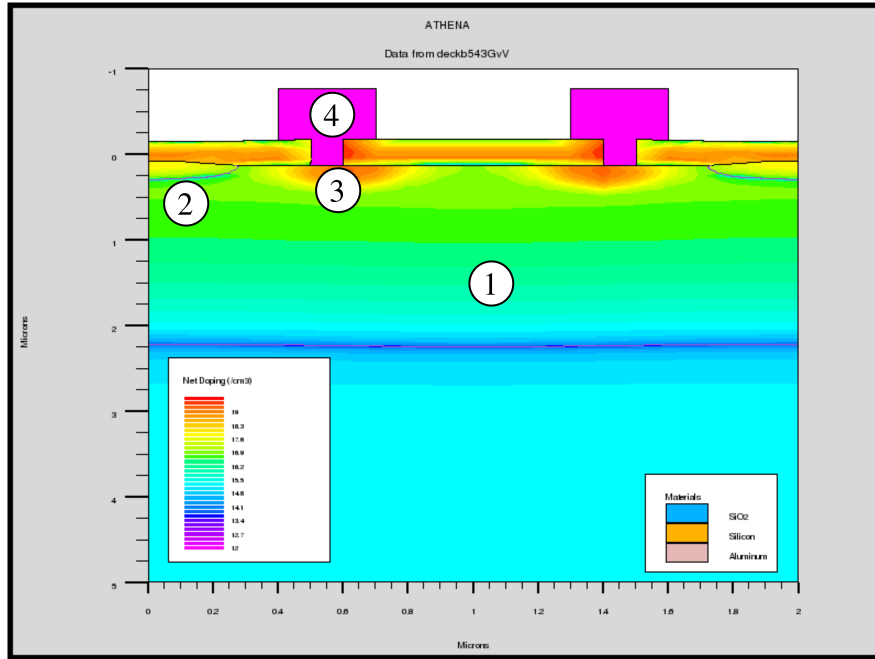

Figure 7: Completed 2-D ATHENA model of Hall effect device showing net doping concentrations throughout the substrate. Key parts of the design are (1) n-well, (2) channel stop, (3) n+ contact, and (4) metal contact.

Figure 7 shows the ATHENA 2-dimensional simulation of a single axis of the completed Hall device and the net doping throughout the n-well region. From this simulation, process parameters such as diffusion times, temperatures, implant energies and dose profiles were optimized. Figure 8 shows a cutline in the above structure through the channel stop region and the boron, phosphorus and net doping concentrations throughout the sample. From the plot it can be seen that there is sufficient boron in the field regions to isolate the two axes on the same chip.

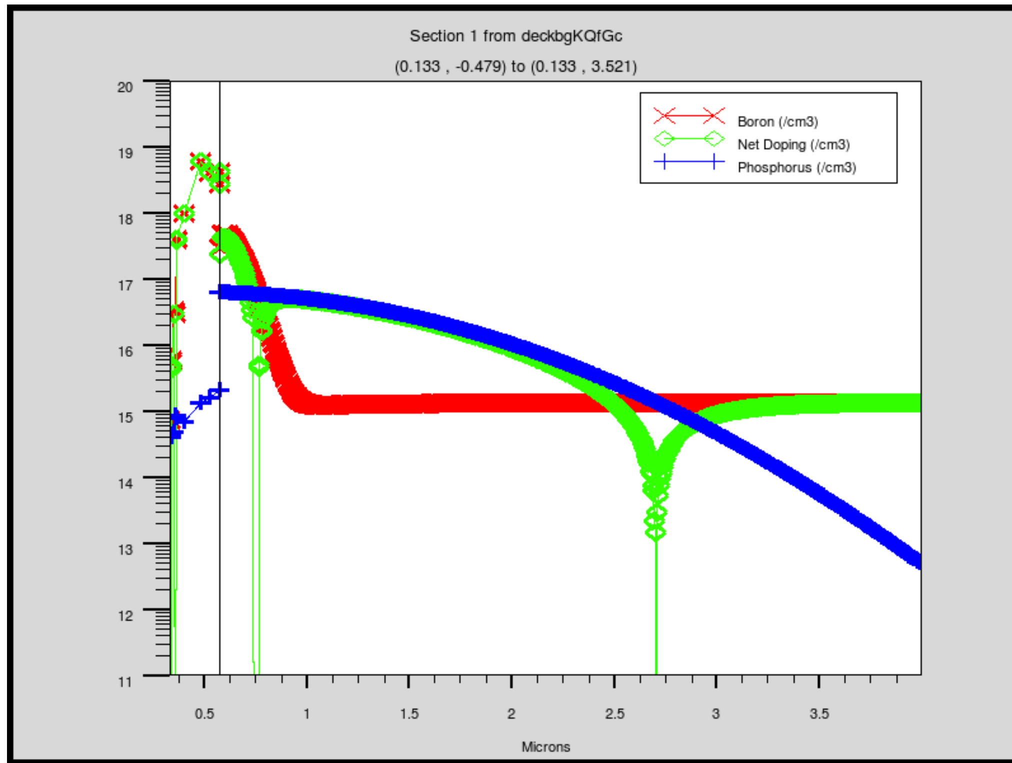

Figure 8: ATHENA plot showing doping concentrations of boron and phosphorus through a cutline in the channel stop implanted area.

<u>Fabrication</u>

Once simulations were complete, fabrication could begin using the processing tools in the RIT Semiconductor Microsystems Fabrication Lab (SMFL). The two axis Hall effect sensor design has approximately 30 process steps to packaging. The entire design is built on 150 mm silicon p-type substrate with a background resistivity of 10 ohm-cm. Figure 9 shows the major process cross-sections and key parameters associated with the processing step

Starting 6” p-type wafer

Coat w/ resist for zero lvl litho
Plasma etch alignment marks

Ash resist and standard RCA clean

Grow 5000 Å masking oxide

Level 1a Lithography – N-well
Etch oxide using 5.2:1 BOE

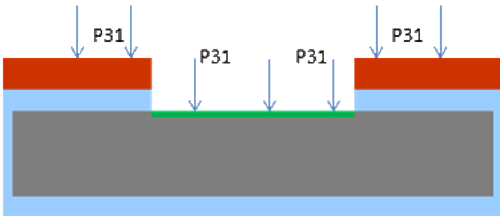

Implant Phosphorus ions
Dose = 9.5E12 cm^{-2} @ 125 KeV

Ash resist and RCA clean

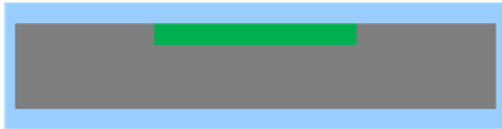

Well drive and 3000 Å oxide growth 1100 °C 330 min N_2 + 25 min O_2

Level 1b Lithography – Channel Stop and Etch oxide using 5.2:1 BOE

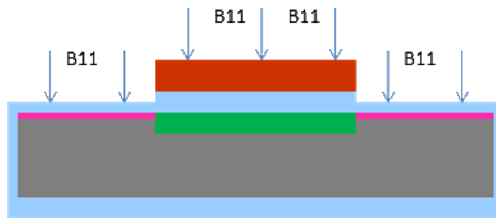

Implant Boron ions
Dose = 1E14 cm^{-2} @ 50 KeV

Ash resist

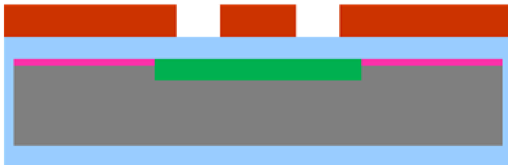

Level 2 Lithography – Contacts

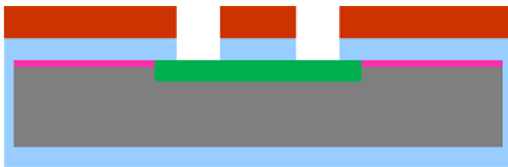

Wet etch contact cuts

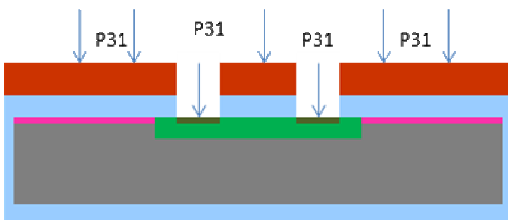

N+ Contact Implant
Dose = 2E15 cm^{-2} @ 60 KeV

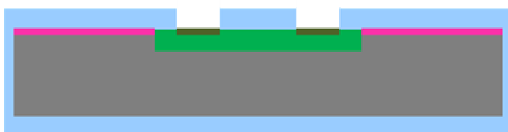

Ash resist

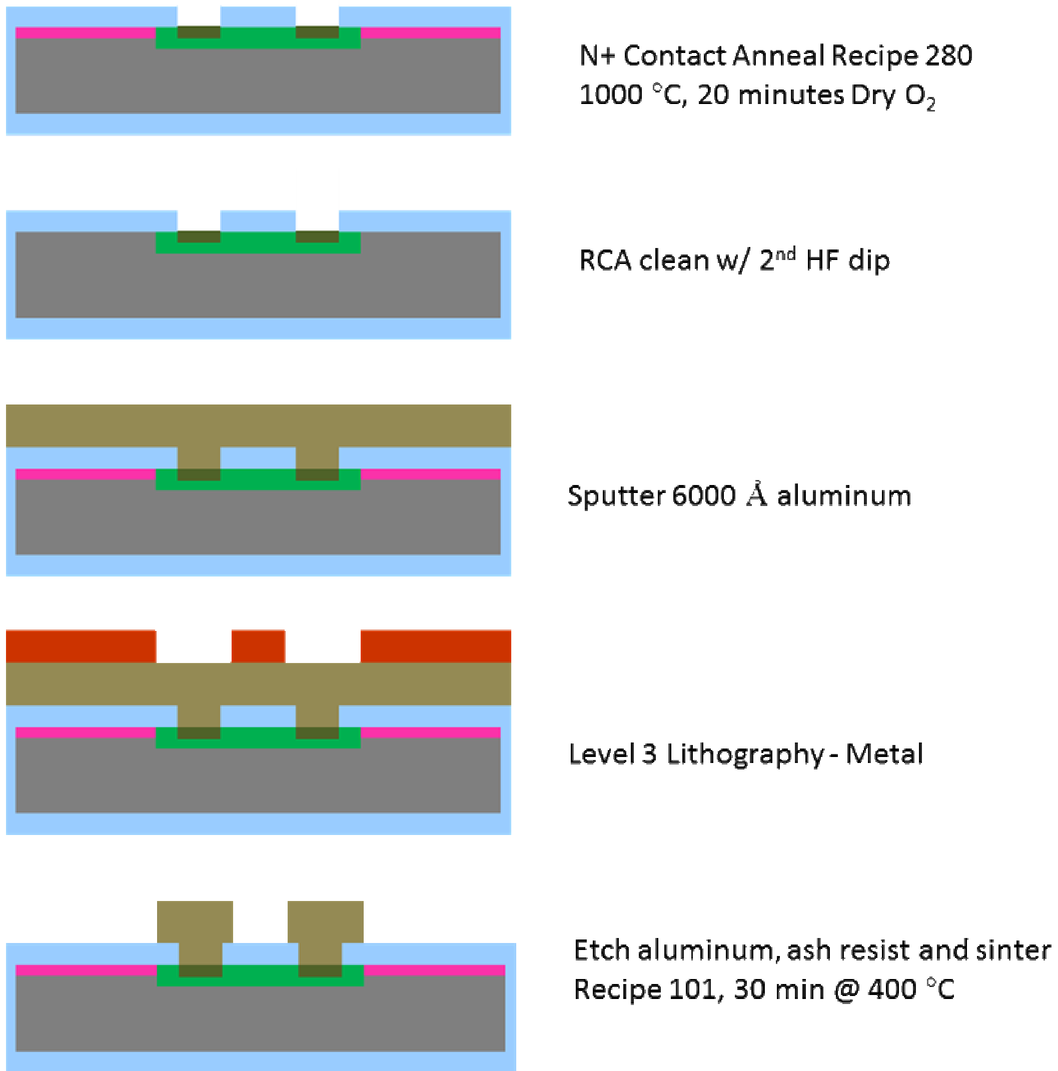

Figure 9: Major process cross-sections including lithography mask layers zero level, n-well, channel stop, contact cuts and metal. Process time usually took 5 – 10 days but could be drastically reduced depending on down tool time.

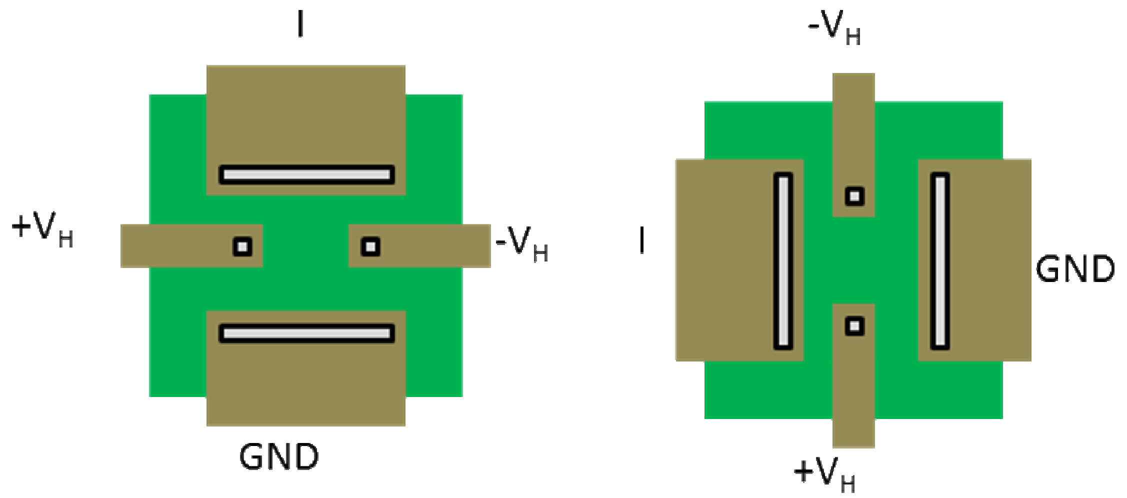

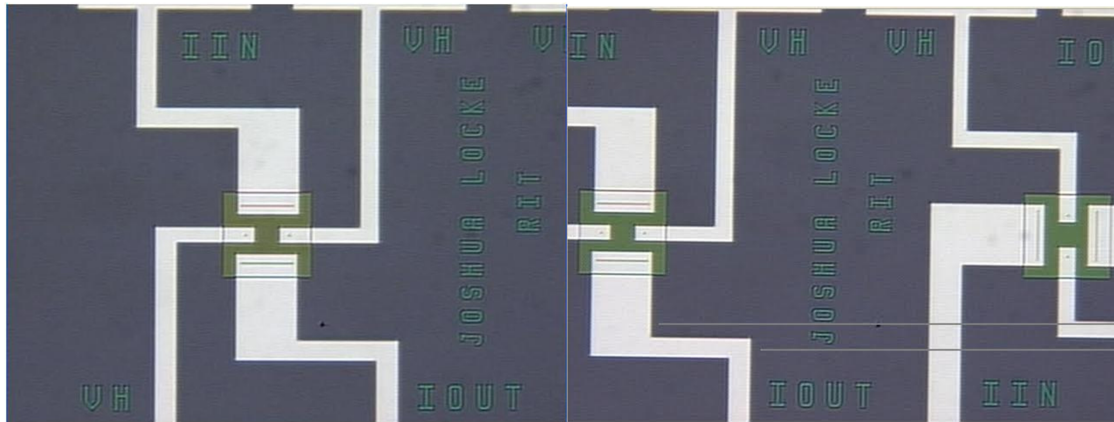

Figure 10: Completed top-down pictorial of the fabricated Hall device (top), a fully processed single axis device (bottom left) and a fully processed two axis device (bottom right).

Packaging

Packaging of the device was done at RIT and started with sawing the wafer into individual 5 mm x 5 mm die using a KS780 Tempress Dicing Saw followed by epoxy bonding to a custom 8 pad PCB. Each 150 mm wafer yields approximately 100 devices. The aluminum sensor pads were then wire bonded to the PCB pads using an Orthodyne Model 20 Ultrasonic Wire Bonder and 1% SiAl wire, 0.003 inches in diameter. The entire chip and bonds are coated with a thin layer of epoxy to protect the sensor and pin strips are soldered to the custom 8 pin PCB to make connections to testing circuitry on a bread board. Figure 11 shows the process steps for packaging the 2-axis Hall effect device described.

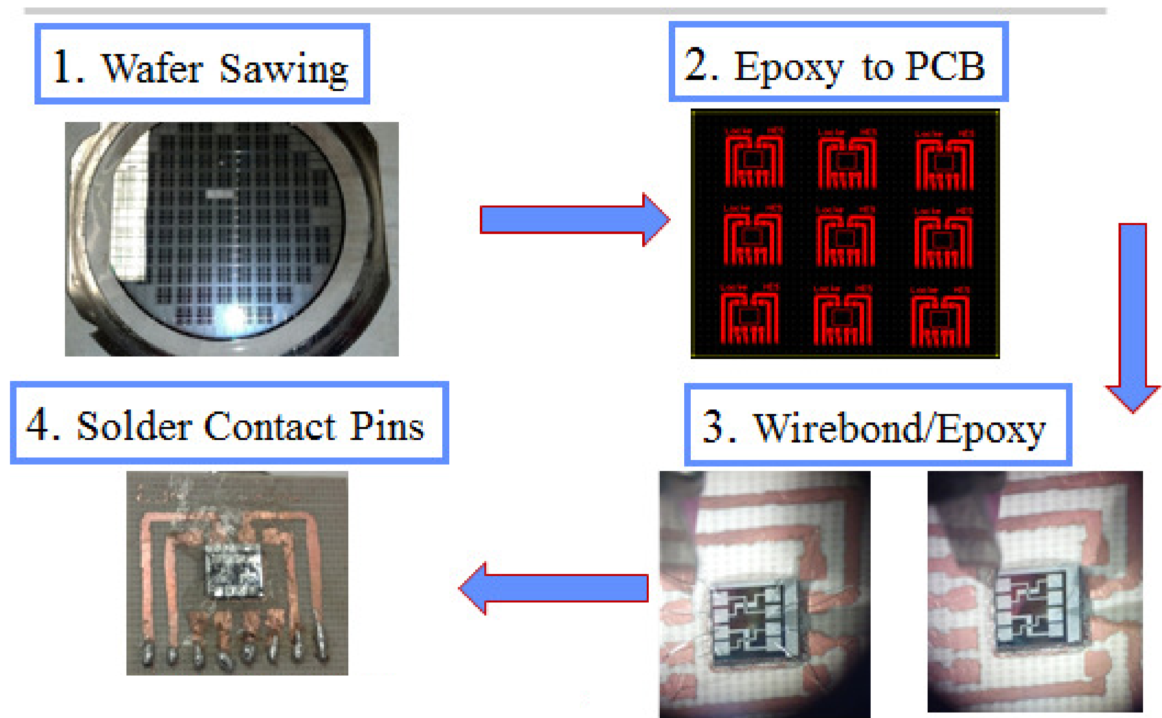

Figure 11: Process steps for packaging 2-axis Hall effect sensor.

Testing

Several testing methods were used to characterize the Hall sensors against known magnetic fields in the form of strong Neodymium (NdFeB) disc magnets. Table 4 shows the magnets used for testing. All surface field values were verified using an Allegro A1326LUA-T low noise, linear Hall effect sensor IC with analog output and a known sensitivity of 2.5 mV/Gauss.

TABLE 4
TESTING MAGNETS

Part #	Dimensions [dia x thick]	Grade -	Surface Field [Gauss]	Pull Force [lbs]
D54-N52	5/16" x 1/4"	N52	6275	6.32
D5H2	5/16" x 2/10"	N42	5201	4.54
D301	3/16" x 1/32"	N42	2087	0.35
D88	1/2" x 1/2"	N42	5903	14.60

The first round of testing was analog testing and was simply placing the magnets on the sensor in the presence of a known current and measuring the resulting Hall voltage. Figure 12 shows the results of a single device with varying magnetic field strength and sensor current. The average sensitivity of the device in Figure 12 at 10 mA supply current is 0.0258 µV/Gauss.

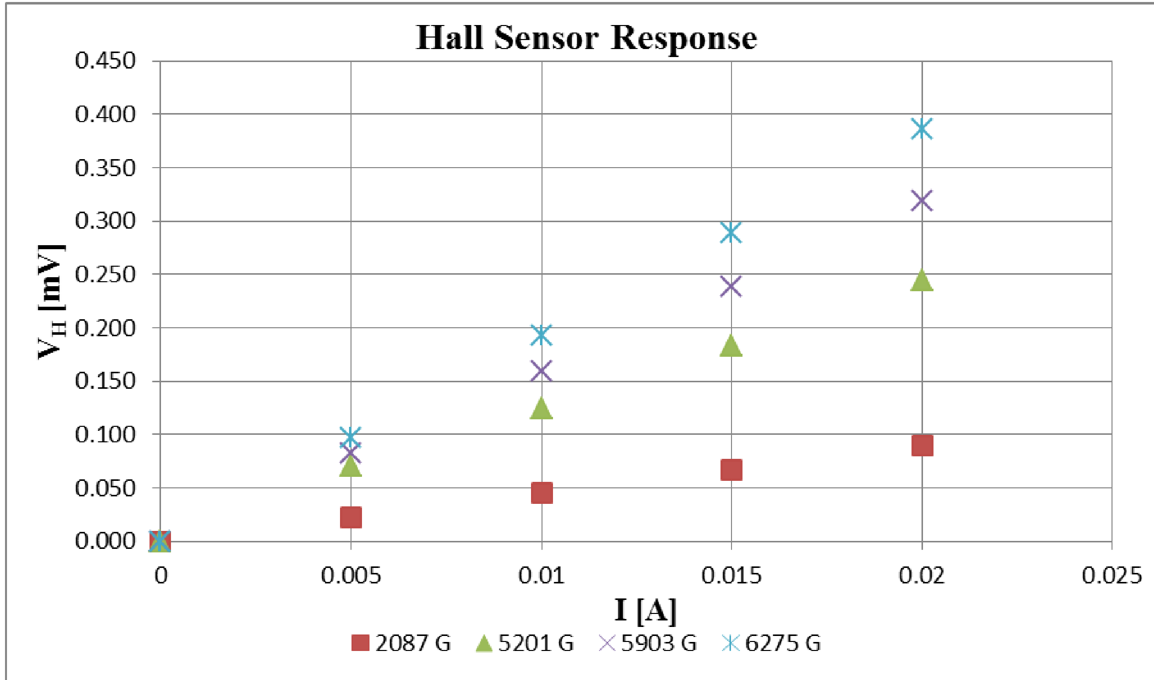

Figure 12: Analog testing results for 2-axis Hall effect sensor with varying large magnetic fields and supply current.

Figure 12 shows that the Hall sensor responded as expected to a changing magnetic field strength by increasing the generated Hall voltage and remained linear with the applied current.

The second round of testing was to verify medium to small magnetic fields using a toroid wound with wire to focus magnetic field lines perpendicular to the sensors. Figure 13 shows the working set-up of a toroid wrapped in wire and Equation 7 shows the flux density of the magnetic field in the toroid gap when a current is applied through the wire where N is the number of turns, I is the current through the wire, μ_R is the relative permeability (taken as 800 for the ferrite core toroid), MPL is the mean path length as shown in figure 13 and L_G is the length of the air gap in the toroid [2].

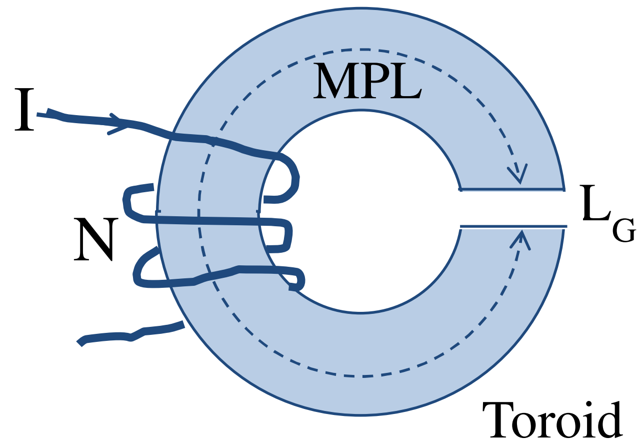

Figure 13: Basic toroid design for generating linear magnetic flux density lines in the air gap when a current is flown through the wire [2].

$$B = \frac{0.4\pi\mu_R NI}{MPL + \mu_R L_G} \quad \text{(eq. 7)}$$

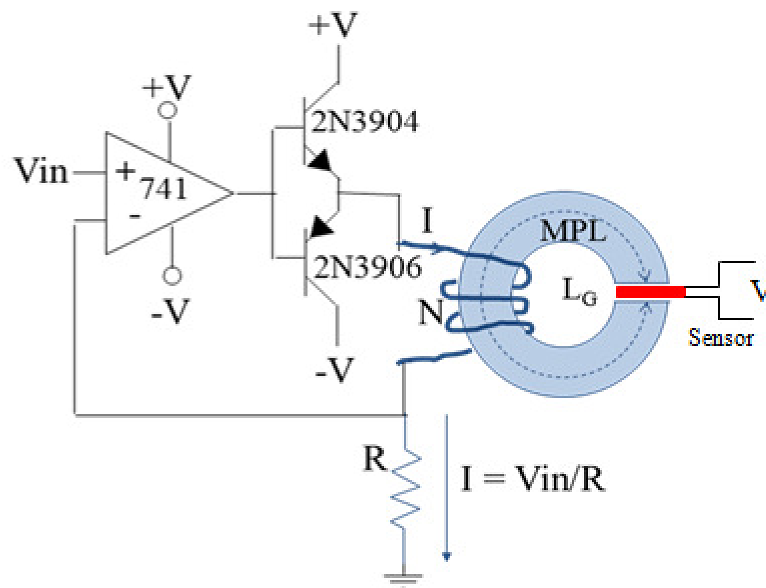

Figure 14: Voltage to current circuit consisting of an LM741 op-amp and NPN and PNP transistors to increase current used to test toroid magnetic flux density. The current provided is equal to Vin/R (R = 10 Ω) [2].

The circuit was tested using the Allegro Hall effect sensor with the results shown in figure 15.

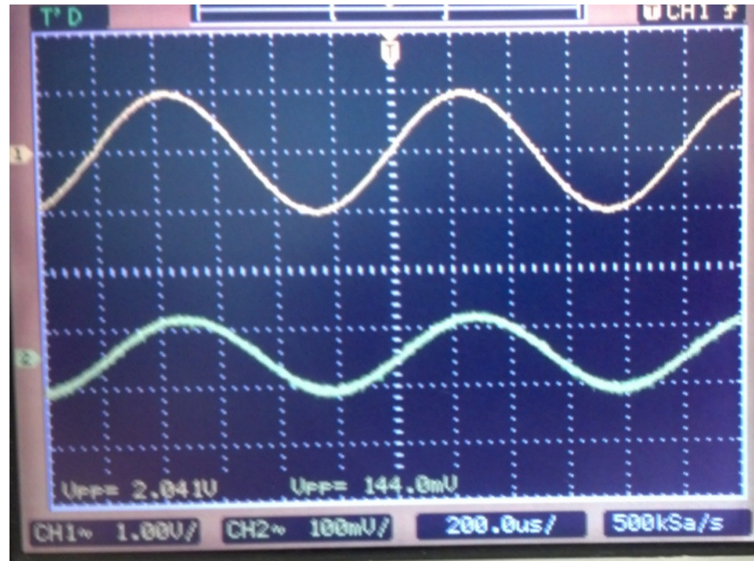

Figure 15: The yellow shows the supplied voltage to the circuit in figure 14. The green is the output signal of the Allegro Hall effect sensor with a $V_{p\text{-}p}$ of 144 mV.

The theoretical output using equation 7 with the supply current of I = 0.204 Amps is B = 50 Gauss and the measured value from the Allegro Hall effect sensor with a sensitivity of S = 2.5 mV/Gass is 56 Gauss making a 13 % error. This shows that the toroid design is capable of making magnetic fields much smaller than the magnets in Table 4. However, when this circuit was used on the new RIT Hall effect design, it was unable to sense the low magnetic field strength due to tremendous noise in the sensor output when the toroid was not present.

While the sensor was ineffective at low magnetic fields, the last form of testing was to accurately determine the magnitude of the strong Neodymium magnets in Table 4. To do this, a high filtered unity gain buffer amplified circuit was constructed to give an accurate

Hall voltage output when a magnet is near. Figure 16 shows the sensor output for both magnetic polarities of the 6275 Gauss neodymium magnet with 11 mA supply current.

Figure 16: Sensor output showing Vmax and Vmin of the hall device in the presence of +6275 G and -6275 G magnetic fields.

Table 5 shows the resultant computed magnetic field strengths versus the measured surface fields of all of the strong magnets and the percent error associated. It can be seen that the sensor is much more accurate at predicting higher magnetic field strengths having a percent error less than 1 for the strongest magnet. This shows that the designed sensor is capable of accurately predicting magnetic field strength with a constant current supplied.

TABLE 5
SENSOR FIELD STRENGTH

Surface Field [Gauss]	Measured [Gauss]	P. Error [%]
6275	6216.6	-0.9
5903	5460.8	-7.5
5201	3573.6	-31.3
2087	2886.9	38.3

Third Axis Design

The fabrication of a third axis Hall effect sensor is proposed. The difficulty of sensing magnetic fields in the z-direction is that the supply current must be run vertically into the silicon substrate so that the Hall voltage can be measured correctly. It is therefore necessary to have a design that allows for voltage to be sensed perpendicular to the applied current passing vertically through the silicon substrate. Fabrication of such a device is more complex than the 2-axis design and furthermore must be optimized to give the maximum Hall voltage available for a given magnetic field strength. The proposed design, seen in Figure 17, makes use of a three layer doped LPCVD polysilicon structure to run current vertically with poly contacts to measure the Hall voltage generated in the presence of a magnetic field. The sensitivity of the device would be less than the 2-axis design as carrier mobility through doped polysilicon is less than that of silicon. The whole design is built over a large isolation n-well and a smaller p-well to allow current to flow from the top contacts into the silicon substrate to be grounded. The whole design uses four metal contacts for supply current, ground and two Hall contacts. This design would be fabricated on a separate substrate as the 2-axis design and packaged with the 2-axis design. It should be noted that this design is only proposed, and would require simulations to optimize prior to fabrication and testing. Figure 17 shows the proposed sensor fabrication steps required.

Starting 6” p-type wafer

Coat w/ resist for zero lvl litho
Plasma etch alignment marks

Ash resist and standard RCA clean

Grow 5000 Å masking oxide

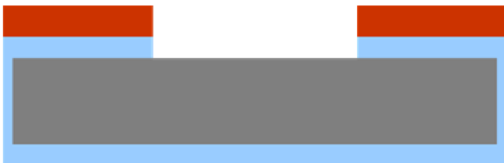

Level 1 Lithography – N-well
Etch oxide using 5.2:1 BOE

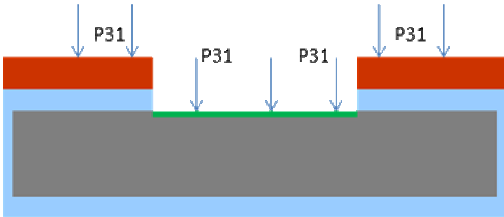

Implant Phosphorus ions

Ash resist and RCA clean

Well drive and oxide growth

Level 2 Lithography – P-well
Etch oxide using 5.2:1 BOE

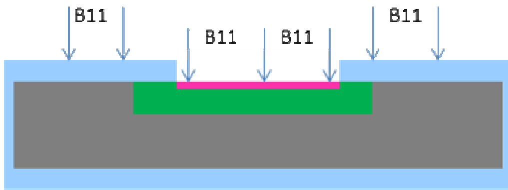

Implant Boron ions

Well drive

Oxide growth

LPCVD – Polysilicon 1

Level 3 Lithography – Poly 1

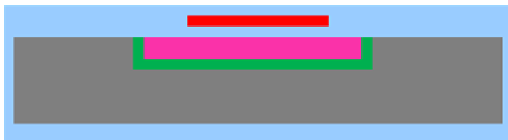

Oxide growth

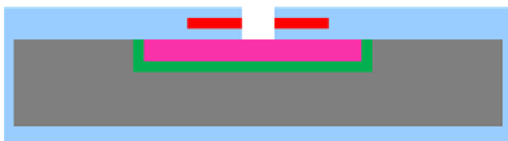

Level 4 Lithography – P-well contact

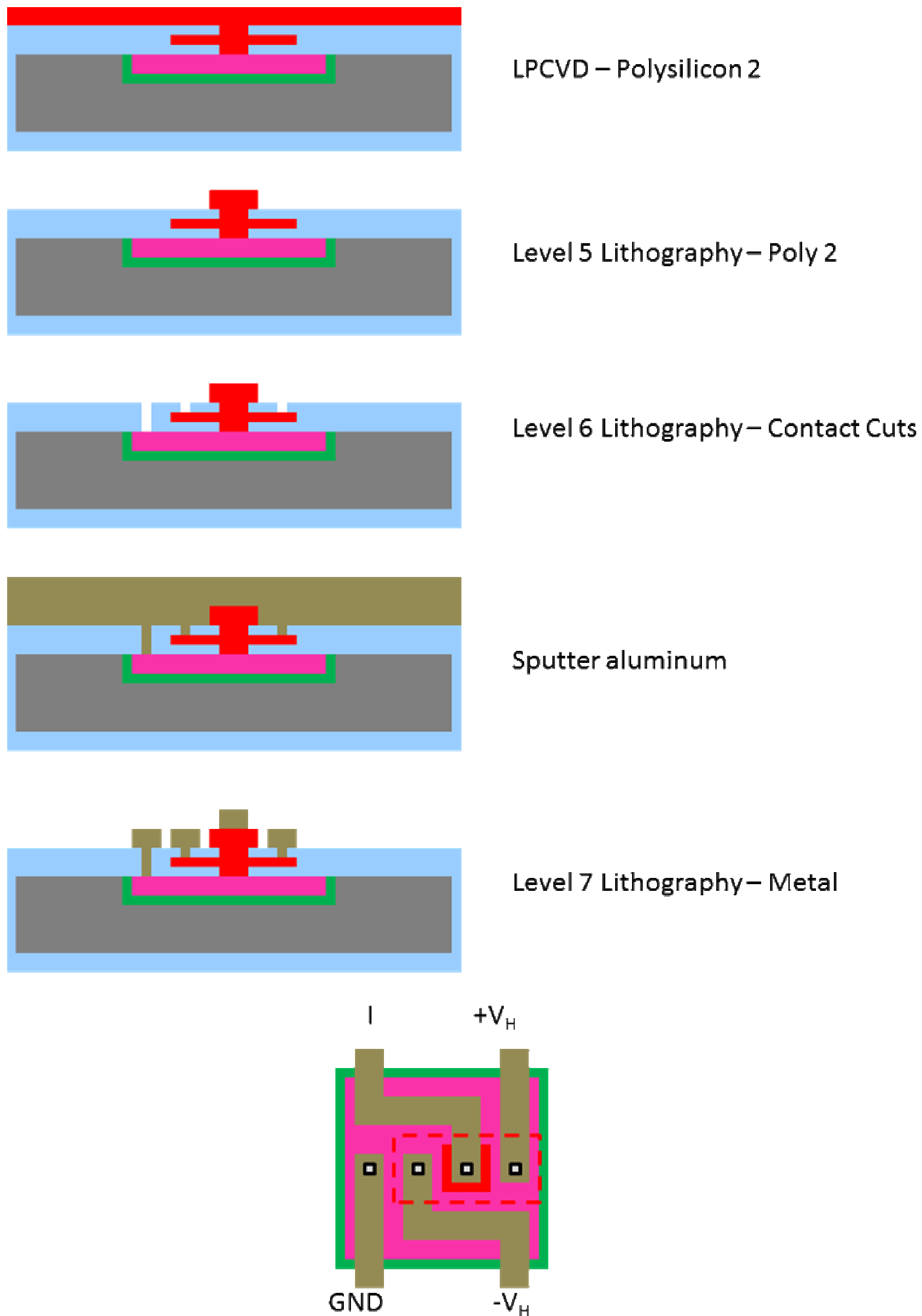

Figure 17: Major process cross-sections for proposed z-axis Hall effect sensor including lithography mask layers and three layer LPCVD polysilicon feature. The top down view shows the four metal contacts for current (I), ground (GND) and two Hall contacts (V_H).

5. CONCLUSION

A 2-axis Hall effect sensor was designed, fabricated, packaged and tested using the RIT sub-CMOS process. The finished design showed sensitivity to strong magnetic fields with a magnitude of 0.0258 μV/Gauss at 10 mA supply current. The designed sensor was unable to sense small magnetic fields due to being unable to concentrate magnetic field lines directly into the sensing n-well. It is also believed that there was a magnetic influence on the sensor caused by small magnetic fields in the device packaging that inhibited the detection of small magnetic fields generated by a toroid. Furthermore, a process for a third axis sensor was proposed but not optimized.

6. REFERENCES

[1] D. Niarchos December 2003 Magnetic MEMS: key issues and some applications Sensors and Actuators A: Physical 109 1-3 166-173 Magnetic MEMS: key issues and some applications

[2] L. Fuller 2013 Hall Effect Sensors 1-43 Hall Effect Sensors

[3] L. Fuller, S. Bhaskaran and I. Phuchades January 2014 RIT's Sub-CMOS Process Rochester Institute of Technology Microelectronics Engineering Department 144 RIT's Sub-CMOS Process http://people.rit.edu/lffeee/SubCmos2014.pdf

[4] R. B. Goldfarb and F. R. Fickett March 1985 Units for Magnetic Properties U.S. Department of Commerce, Colorodo 80303 National Bureau of Standards Units for Magnetic Properties

[5] M.-A. Paun, J.-M. Sallese and M. Kayal 2010 Geometry Influence on the Hall Effect Devices Performance U.P.B. Sci. Bull 72 4 257-271 Geometry Influence on the Hall Effect Devices Performance 1223-7027

[6] D. B. Pengra, J. Stoltenberg, R. Van Dyck and O. Vilches 2007 Hall Effect 1-10 Hall Effect

[7] R. S. Popovic 2004 Hall Effect Devices Institute of Physics Publishing Second Edition Hall Effect Devices

[8] E. Ramsden February 2006 Hall-Effect Sensors: Theory and Application Burlington, MA, USA Newnes 265 2nd Hall-Effect Sensors: Theory and Application

[9] P. Ripka and M. Janošec June 2010 Advances in Magnetic Field Sensors IEEE Sensors Journal 10 6 1108-1116 Advances in Magnetic Field Sensors